Geometric scaling of purely-elastic flow instabilities

J. Zilz[1], R. J. Poole[2], M. A. Alves[3], D. Bartolo[1], B. Levaché[1] and A. Lindner[1]
[1] *PMMH UMR7636-ESPCI Paristech-CNRS-Paris 6-Paris 7, 10, rue Vauquelin F-75231 Paris Cedex 05, France.*
[2] *School of Eng., University of Liverpool, Brownlow Hill, Liverpool, L69 3GH, UK.*
[3] *CEFT, DEQ, FEUP, Rua Dr. Roberto Frias, 4200-465 Porto, Portugal*
(Dated: September 26, 2011)

We present a combined experimental, numerical and theoretical investigation of the geometric scaling of the onset of a purely-elastic flow instability in a serpentine channel. Good qualitative agreement is obtained between experiments, using dilute solutions of flexible polymers in microfluidic devices, and two-dimensional numerical simulations using the UCM model. The results are confirmed by a simple theoretical analysis, based on the dimensionless criterion proposed by Pakdel-McKinley [1, 2] for onset of a purely-elastic instability.

PACS numbers: 47.50.-d, 47.61.-k, 47.20.Gv

Purely-elastic flow instabilities occur for low Reynolds number flows of viscoelastic fluids. Such elastically-driven instabilities - which are entirely absent for the equivalent Newtonian fluid flow - have been experimentally observed in a range of macroscopic flow geometries such as viscometric Couette or plate-plate devices [3, 4]. The onset of instability has been attributed to a balance between normal stresses and streamline curvature [4]. Pakdel and McKinley (Pak-McK) [1, 2] proposed an elegantly simple dimensionless criterion to unify the experimental observations up to that date. However, beyond the lid-driven cavity results used in [1], systematic studies of the instability threshold as a function of the curvature of a given flow are still lacking. In this Letter we investigate the geometric scaling of the onset of a purely-elastic instability in serpentine channels of rectangular cross-section, combining experiments, numerical simulations and a simple theoretical analysis. In such wavy channels the geometric influence on the curvature is dominant and the curvature is essentially independent of flow rate. A major complication of investigating curvature effects in most other complex flows - e.g. abrupt contractions or lid-driven cavity flows - is that the dominant flow curvature is not solely determined geometrically but by the precise dynamics of the flow itself (e.g. varying locally and with flow rate). These elastic instabilities have proven to be a good way to obtain efficient mixing in microfluidic devices [5]. Newtonian fluid flow in microfluidic devices occurs typically in the laminar regime, due to the characteristic small length scales, and mixing occurs primarily via diffusion, a very slow process. However, the addition of small amounts of flexible polymers with high molecular weight is sufficient to impart strong non-Newtonian behavior, and can even lead to so-called "elastic turbulence" [6], with increased flow resistance and enhanced mixing performance [7]. It is thus of great importance to understand the underlying mechanism that leads to the onset of instability and test the robustness of the Pak-McK criterion.

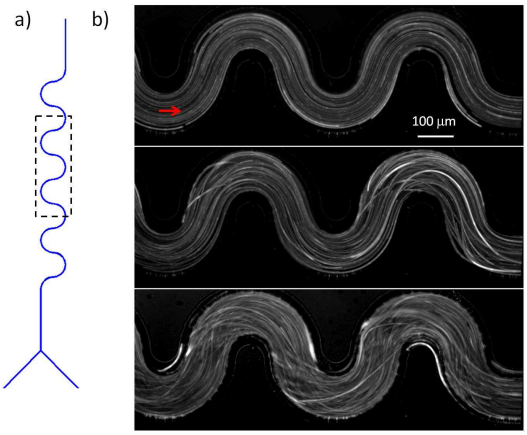

FIG. 1: Sketch of the microchannel; typical *instantaneous* flow patterns in a dilute solution of PEO. From top to bottom: stable flow; slightly unstable flow (close to onset of elastic instability); unstable flow.

We use microfluidic devices, which are important in applications such as lab-on-a-chip, fabricated in polydimethylsiloxane (PDMS) from an SU-8 mould, using standard soft-lithography techniques, which allow straightforward variation of the flow geometry. Furthermore, due to the small dimensions of the channel, high shear rates are easily achievable, thus enhancing the non-Newtonian behaviour observed, while keeping inertia small. The experiments were performed in serpentine channels with varying radii of curvature and channel dimensions, using dilute solutions of a flexible polymer in different solvent viscosities. The onset of a purely-elastic instability (see Fig. 1) was investigated as a function of the relaxation time of the flexible polymer solution and the geometrical characteristics of the channel (radius and width). Two-dimensional (2D) numerical simulations are performed using the upper-convected Maxwell (UCM) model in identical geometries, assuming that the curvature in the 2D base-flow is responsible for the insta-

bility (preliminary 3D calculations confirmed the appropriateness of this approach). The combination of both approaches, together with a simple theoretical analysis, based on the Pak-McK criterion, allowed us for the first time to predict the geometric scaling of the onset of a purely-elastic instability in curved channel flow. In addition our results independently confirm the strength of the Pak-McK criterion and open the possibility for extending similar analyses to a range of other flows.

The geometry of the serpentine channels used in this study are represented in Fig. 2(a) (simulations) and in Fig. 1 (experiments). The flow takes place through a given number of half loops in a channel of width W (and height H) and inner radius R. In the straight parts of the inlet and outlet the velocity profile can be estimated using the analytical solution for fully-developed flow in a rectangular channel, valid for fluids with a constant shear viscosity (either Newtonian or viscoelastic). In the curved parts of the channel the flow becomes weakly asymmetric and the maximum velocity location occurs slightly closer to the inner wall. In between the two half loops the flow regains symmetry, before becoming asymmetric towards the other side in the next half loop. The asymmetry becomes less pronounced with increasing dimensionless radius R/W. The flow is mainly shear dominated, as can be seen on the contour plot of the flow-type parameter shown in Fig. 2b (from simulations), with limited regions of elongational and rotational flows close to the centreline where the deformation rates are small. The flow-type parameter is defined as $\xi = \frac{|\mathbf{D}|-|\mathbf{\Omega}|}{|\mathbf{D}|+|\mathbf{\Omega}|}$, where $|\mathbf{D}|$ and $|\mathbf{\Omega}|$ represent the magnitudes of the rate of deformation and vorticity tensors [8], and varies from $\xi = -1$ (solid-like rotation), up to $\xi = 1$ (extensional flow). A shear-dominated region is identified where $\xi = 0$. We define the average shear rate as $\dot{\gamma} = U/W$, with U representing the average velocity in the channel. The Reynolds number is here defined as $\mathrm{Re} = \rho UW/\eta$, with ρ and η representing the density and shear viscosity of the fluid, respectively. The Weissenberg number is defined as $\mathrm{Wi} = \lambda\dot{\gamma}$, where λ is the relaxation time of the fluid. While Re quantifies the relative importance of inertial over viscous forces, the degree of elasticity of the flow is quantified using Wi (ratio of elastic to viscous stresses).

The experiments were performed in serpentine microchannels composed by eight half loops (Fig. 1(a)). We work with channels of different width, $W = 60$ and 100 µm, but keep the aspect ratio $a = W/H$ nearly constant and close to 1.4, a typical aspect ratio for microfluidic devices. The radius of curvature was varied from R=25 to 1950 µm, in such a way that for each channel width the dimensionless radius R/W varies approximately from 0.5 to 20.

Solutions of the flexible polymer PEO (Sigma Aldrich) with a molecular weight, $M_w = 2 \times 10^6$ g/mol, at a concentration of 125 ppm (w/w) were used in water/glycerol mixtures. The overlap concentration is $c^* \simeq 860$ ppm [9] and we thus work in the dilute limit. The solvent viscosity η_s varies from $\eta_s = 0.93$ mPa.s to 7.4 mPa.s for varying concentrations of glycerol at 23°C. For these solutions the polymer viscosity η_p is approximatively 13% of the solvent viscosity, η_s, as measured with a Ubbelohde viscometer. We have also measured the flow curves of the polymer solutions (not shown) and no shear thinning is observed. For such small concentrations it is very difficult to measure the relaxation time directly [10], therefore we estimated λ from the Zimm relaxation time. Since the flow in the serpentine channel is shear dominated, the use of a relaxation time linked to shear is the most appropriate. From Rodd *et al.* [9] we have calculated the Zimm relaxation time for PEO of $M_w = 2 \times 10^6$ g/mol at 23°C in water to be $\lambda = 0.36$ ms. We have fitted the dependence of the Zimm relaxation time on the solvent viscosity η_s as found by Rodd *et al.* [9] (see also [11]) using a power law equation, $\lambda = 0.4\eta_s^{0.7}$, with λ given in ms and η in mPa.s, and use this equation to estimate the relaxation times of all the solutions used in the experiments.

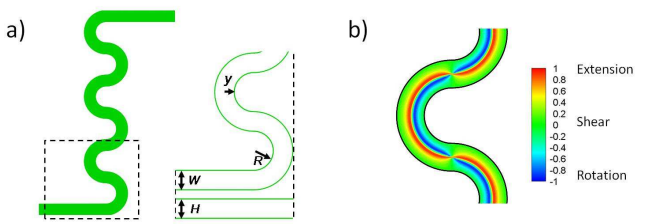

FIG. 2: a) Geometry and definitions (*note*: the y-direction points to the center along any radial line through each half loop); b) flow-type parameter.

The experimental protocol can be summarized as follows. The solutions are fed to the channel via two inlets, and one of them is fluorescently dyed. In this way we can visually assess the stability of the flow. The flow rate (Q) was varied from 1 to 50 µl/min, and is imposed via a syringe pump (PHD 2000, Harvard apparatus). The flow is visualized using an inverted microscope (Axio Observer, Zeiss) coupled to a CCD camera. Starting with the lowest flow rate, Q is then gradually increased. After each change in Q we wait a sufficiently long time to achieve steady-state flow conditions (on the order of 10 minutes). The onset of fluctuations in the flow is monitored at the last loop of the serpentine channel. This critical condition defines the onset of the time-dependent elastic instability, and the critical flow rate Q_c is determined. For each experimental condition two separate runs are performed using freshly prepared polymer solutions. We have also visualized the onset of instability using fluorescent micro-particles (see Fig. 1(b)).

A systematic study was undertaken to determine the

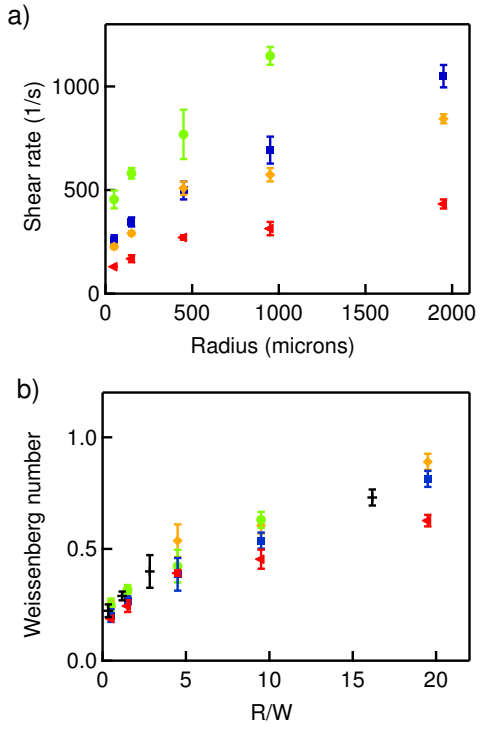

FIG. 3: Threshold of instability in a channel of width $W = 100$ µm and $H = 80$ µm for a solution of 125 ppm of PEO ($M_w = 2 \times 10^6$ g/mol) with different solvent viscosities η_s (1.8 mPas (●), 2.8 mPas (■), 4.5 mPas (♦), 7.4 mPas (◀)) and $W = 60$ µm and $H = 40$ µm (0% of glycerol (–)) (a) Critical shear rate $\dot{\gamma}_c$ as a function of the radius R. (b) Critical Weissenberg number Wi_c as a function of R/W.

critical flow rate for onset of an elastic instability as a function of the radius of curvature of the channel, R, the width of the channel, W, and the relaxation time of the polymer solutions, λ. The critical shear rate, $\dot{\gamma}_c = Q_c/(HW^2)$, was determined as a function of R, for a first set of channels of width $W = 100$ µm and height $H = 80$ µm, using different solvent viscosities. The results are depicted on Fig. 3 (a) from which it is clear that $\dot{\gamma}_c$ increases with R. Additionally, one can observe that the critical shear rate is higher for lower solvent viscosities. The critical Weissenberg number, $\mathrm{Wi}_c = \lambda\dot{\gamma}_c$, is represented in Fig. 3 (b) as a function of R/W. A reasonably good scaling of the data is obtained for all sets of experiments. Additionally, the data from another set of channels ($W = 60$ µm, $H = 40$ µm) are also depicted on Fig. 3 (b) for selected solvent viscosities. Good agreement between the different channel sizes is obtained, therefore confirming that Wi_c is a function of R/W. The Reynolds numbers for the various experiments presented on Fig. 3 vary from 0.2 to 5, therefore, although small, inertial effects are not negligible. However, we do not observe a modification of the Wi_c threshold as a function of Re (largest for the small solvent viscosities). For the smallest solvent viscosity and a channel of radius $R = 1950$ µm, the flow does not become unstable in the range of flow rates accessible in the experiments, and we attribute this behaviour to a stabilizing effect due to inertia for $\mathrm{Re} > 5$ (as also observed in [12]).

For simplicity, the numerical simulations assume 2D planar flow of an incompressible viscoelastic fluid described by the UCM model. The equations that need to be solved are those of mass conservation, $\nabla \cdot \mathbf{u} = 0$, and the momentum equation, $-\nabla p + \nabla \cdot \boldsymbol{\tau} = \mathbf{0}$, assuming creeping-flow conditions (i.e. the inertial terms are exactly zero). The evolution equation for the extra-stress tensor, $\boldsymbol{\tau}$, is given by $\boldsymbol{\tau} + \lambda\boldsymbol{\tau}_{(1)} = \eta\dot{\boldsymbol{\gamma}}$, where $\boldsymbol{\tau}_{(1)}$ represents the upper-convected derivative of $\boldsymbol{\tau}$. Despite the well-known shortcomings of this simplified model, such as the unbounded nature of the steady extensional stresses above a critical strain rate ($\lambda\dot{\epsilon} = 0.5$), it is the simplest differential constitutive equation which can capture qualitatively many features of highly-elastic flows. In addition it forms the backbone of many more complex models (e.g. the FENE-P, Giesekus and Phan-Thien–Tanner models), which simplify to the UCM in certain parameter limits, and thus it is extremely general. The governing equations are solved using a fully implicit finite-volume numerical method, based on the logarithm transformation of the conformation tensor, as described in detail in [13] and references therein.

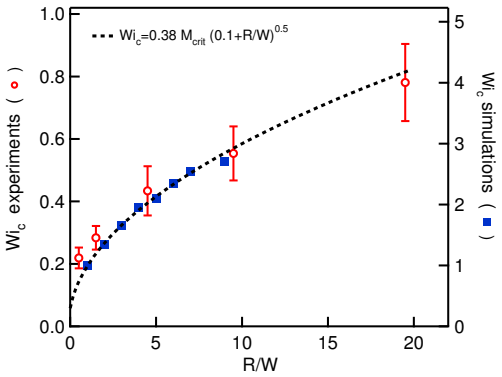

FIG. 4: Comparison of experimental and numerical results, with the scaling analysis based on Pak-McK criterion. The experimental data are the average over the results presented in Fig. 3 (b) for the channel of width $W = 100$ µm.

Fig. 4 displays the average Wi_c, and the corresponding standard deviation, of the experimental data, together with the predictions from the numerical simulations, as a function of R/W. Wi_c for the simulations reflects the highest Wi for which a steady solution could be obtained. In the experiments the ratio η_p/η_s is constant and we can thus expect qualitative agreement between the experimental data and the results from the simulations using the UCM model. This is indeed the case and good qualitative agreement between experiments and simulations is obtained.

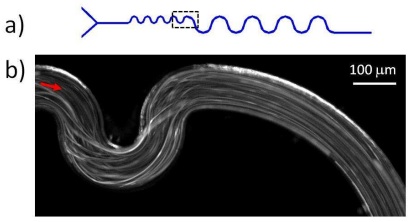

FIG. 5: a) Sketch of the modified channel; b) streak photography for a dilute solution of PEO: the flow is unstable in the part of the channel with small radius ($R = 50$ µm), but stable in the part with the large radius ($R = 450$ µm).

Pakdel and McKinley [1, 2] showed that the curvature of the flow and the tensile stress acting along the streamlines could be combined in the form of a dimensionless criterion that must be exceeded for the onset of purely elastic instability: $\left[\frac{\tau_{11}}{\eta\dot{\gamma}}\frac{\lambda u}{\mathcal{R}}\right] \geq M_{crit}^2$ with $\mathcal{R}$, u and $\dot{\gamma}$ representing the local streamline curvature, velocity and shear rate, respectively. τ_{11} represents the local streamwise normal stress and $\eta\dot{\gamma}$ the local shear stress. For the UCM model the normal stress can be written as $\tau_{11} = 2\eta\lambda\dot{\gamma}^2$. Assuming fully-developed flow conditions everywhere (below Wi_c), we can estimate the velocity profile assuming a Poiseuille flow, $u = \frac{3}{2}U[1 - (\frac{y}{W/2})^2]$, with the y-axis centred on the channel and directed along any radial line through each half loop towards the centre. The shear rate is given as $\dot{\gamma} = 12U|y|/W^2$, therefore one obtains the following criterion for a purely-elastic instability, $36(\frac{\lambda U}{W})^2 F(y) \geq M_{crit}^2$, where $F(y) = \frac{|\frac{y}{W}|[1-4(\frac{y}{W})^2]}{\frac{R}{W}+\frac{1}{2}-\frac{y}{W}}$. For each value of R/W we can determine the location where the onset of the instability takes place, which occurs at y_c/W where $F(y_c)$ is maximum. Therefore, for each value of R/W we can also determine the corresponding Wi_c for onset of instability. In general this has to be done numerically, but for the limits of very low and very high values of R/W this can be done analytically, leading to the following asymptotes and critical locations:

(i) $\mathrm{Wi}_c \to \frac{M_{crit}}{\sqrt{72}}$; $y_c/W \to \frac{1}{2}$ for $\frac{R}{W} \to 0$

(ii) $\mathrm{Wi}_c \to 0.38 M_{crit}\sqrt{\frac{R}{W}}$; $y_c/W \to 0.289$ for $\frac{R}{W} \to \infty$

These asymptotes can be combined in the general form, $\mathrm{Wi}_c = 0.38 M_{crit}\sqrt{0.1 + \frac{R}{W}}$, which agrees well in the whole range of R/W with the exact results that are obtained by solving numerically the general equation derived from the Pak-McK criterion. When fitting the data with this expression, one obtains $M_{crit} = 2.46$ and 0.48 for the simulations and the experiments, respectively. The comparison of the results from experiments, simulations and the scaling argument thus show that Wi_c at the onset of elastic instability in a serpentine channel scales as the square root of R/W with a small offset when R/W tends towards zero.

We have also tested the nature of the instability in the experiments. First we have shown that increasing or decreasing Q does not lead to different values of Wi_c and no hysteresis is observed. Second, we have perturbed the flow at the inlet using a modified serpentine channel composed of a series of loops of small radius 50 µm $< R_1 <$ 250 µm, followed by a serpentine channel of larger radius, $R_2 = 450$ µm (see Fig. 5). No modification of the threshold in the second serpentine channel is observed when varying the radius of the first channel. The streak image shown in Fig. 5 was taken at a flow rate where the flow in the first channel is unstable whereas the flow in the second channel is stable. One observes a fast decay of the perturbation once the fluid enters the second channel. We thus conclude that the instability in the serpentine channel is supercritical in contrast to observations made in Couette or plate-plate devices [14].

Using a combined experimental and numerical approach we investigated the geometrical scaling of a purely-elastic instability in a serpentine channel. In this way we have shown that the critical Weissenberg number at the onset of the instability scales as the square root of the inner radius divided by the width of the channel, R/W, with a small offset when $R/W \to 0$, in agreement with a simple theoretical analysis based on the dimensionless criterion of Pakdel-McKinley [1, 2].

Acknowledgements – We thank A. Morozov and B. Andreotti for useful discussions, A. Morozov for a critical reading of the manuscript and P.C. Sousa for rheological measurements.

[1] P. Pakdel and G. H. McKinley, Phys. Rev. Letters **77**, 2459 (1996).
[2] G. McKinley, P. Pakdel, and A. Oztekin, J. Non-Newt. Fluid Mech. **67**, 19 (1996).
[3] R. G. Larson, E. S. G. Shaqfeh, and S. J. Muller, J. Fluid Mech **218**, 573 (1990).
[4] E. S. G. Shaqfeh, Ann. Rev. Fluid Mech. **28**, 129 (1996).
[5] A. Groisman and V. Steinberg, Nature **410**, 905 (2001).
[6] A. Groisman and V. Steinberg, Nature **405**, 53 (2000).
[7] B. Thomases and M. Shelley, Phys. Rev. Lett. **103**, 094501 (2009).
[8] J. Lee, R. Dylla-Spears, N.-P. Teclemariam, and S. Muller, Applied Physics Letters p. 074103 (2007).
[9] L. E. Rodd, J. J. Cooper-White, D. V. Boger, and G. H. McKinley, J. Non-Newt. Fluid Mech. **143**, 170 (2007).
[10] A. Lindner, J. Vermant, and D. Bonn, Physica A **319**, 125 (2003).
[11] A. Zell, S. Gier, S. Rafai, and C. Wagner, J. Non-Newt. Fluid Mech. **165**, 1265 (2010).
[12] R. J. Poole, M. A. Alves, and P. J. Oliveira, Phys. Rev. Letters **99** (2007).
[13] A. Afonso, P. J. Oliveira, F. T. Pinho, and M. A. Alves, J. Non-Newt. Fluid Mech. **157**, 55 (2009).
[14] A. N. Morozov and W. van Saarloos, Physics Reports **447**, 112 (2007).